ELSEVIER

Thermochimica Acta 356 (2000) 27–38

thermochimica acta

www.elsevier.com/locate/tca

Liquid–solid phase transformation of $C_{16}H_{34}$, $C_{28}H_{58}$ and $C_{41}H_{84}$ and their binary and ternary mixtures

Irena Paunovic, Anil K. Mehrotra*

Department of Chemical and Petroleum Engineering, University of Calgary, Calgary, Alta., Canada T2N 1N4

Received 7 January 2000; received in revised form 15 March 2000; accepted 15 March 2000

Abstract

Differential scanning calorimetry (DSC) was used to study the phase transformations of three pure *n*-alkanes, namely hexadecane ($C_{16}H_{34}$), octacosane ($C_{28}H_{58}$) and hentetracontane ($C_{41}H_{84}$), and their binary and ternary mixtures. The DSC results were used to investigate the liquid–solid phase equilibrium of *n*-alkane mixtures, all of which show eutectic behavior. The experimental liquid–solid phase transformation temperatures were compared with predictions obtained from available eutectic equilibrium models. The results show the presence of non-idealities in all of the mixtures. © 2000 Elsevier Science B.V. All rights reserved.

Keywords: *n*-Alkanes; Mixtures; Eutectic systems; DSC

1. Introduction

The precipitation and deposition of paraffin waxes from crude oils is a commonly observed phenomenon in the production of petroleum products. Typically, paraffin waxes are a mixture of *n*-alkanes and constitute about 40–60% of average crude oil deposits. Wax precipitation is undesirable because it causes plugging of pipelines, reservoirs and process equipment. This problem has been recognized for many years, and a number of studies have investigated the causes and means of preventing the wax precipitation and deposition problems. A variety of mechanical (e.g. pigging), thermal (e.g. heat tracing) and chemical (e.g. use of pour point depressants) treatments have been developed over the years to alleviate the problems associated with wax deposition as well as pipeline transportation problems, which include heating-cooling cycles, water emulsions and crystal modifiers.

Paraffin precipitation is an example of fluid–solid phase equilibrium, which is a result of changes in the 'solvent capacity', temperature changes in the wellbore, pressure and temperature changes in the equipment and pipelines. Wax deposition mechanisms need to be more thoroughly understood in order to make better economic decisions concerning the modern approach to petroleum reservoir development, production system design for primary production, and enhanced recovery [1].

A wide variety of experimental techniques and approaches have been used to study the crystallization behavior of paraffin waxes. Properties of crude oils, such as thermal behavior, kinetics of crystallization, rheological properties, structural characteristics, etc.

* Corresponding author. Tel.: +1-403-220-7406; fax: +1-403-284-4852.
E-mail address: mehrotra@ucalgary.ca (A.K. Mehrotra)

PII: S0040-6031(00)00503-7

have been investigated using differential scanning calorimetry (DSC), infrared spectroscopy, X-ray diffraction, dilatometry, electron crystallography, thermomicroscopy, nuclear magnetic resonance (NMR) and gas chromatography [2–9].

In order to successfully formulate the mathematical description of wax melting and solidification, it is important to know exactly how these mixtures melt in relation to the pure components. Binary and ternary mixtures of *n*-alkanes serve as important model systems for understanding not only wax solidification, but also for the investigation of the effect of chain-length non-homogeneities on the properties of complex chain-molecules such as polymers and lipid bilayers [10].

When two members of the same homologous series of compounds are blended together, they may form systems representative of two extreme cases involving either complete solubility (isomorphous solution) or nearly complete insolubility (eutectic mixture). Kitaigorodskii [11] established the rules and conditions that would favor the formation of stable solid solutions. It was reported that the co-solubility of alkanes in the solid state is sensitive to the relative molecular volumes of the two components making up the binary mixture and their respective crystal structure symmetries. Matheson and Smith [12] proposed an empirical rule, which defines the boundary conditions or limits for continuous solid solutions in mixtures of alkanes. The boundary conditions for the formation of solid solutions of *n*-alkanes were prescribed by the following relationship:

$$n_{\max} = 1.244 n_{\min} - 0.411 \quad (1)$$

Using a Gibbs free energy analysis, Bhat [13] developed a more theoretical relationship for the miscibility limits

$$n_{\max} = 1.16 n_{\min} + 2.07 \quad (2)$$

Dirand et al. [14] presented a comprehensive study on binary mixtures and solid solutions. In spite of what is generally found in the literature [3,6,7,15,16], two consecutive even–even or odd–odd *n*-alkanes do not form a continuous homogeneous solid solution; instead, they form terminal solid solutions that have the pure *n*-alkane structure and many intermediate solutions. Recently, Coutinho and Meray [17] presented a new experimental DSC technique to establish solid–liquid equilibrium phase diagrams of binary systems of organic compounds with complete immiscibility in solid phase. The technique measures the changes on the relative size of the liquid phase during the fusion of a mixture, which is later converted into phase diagrams using the lever rule. Chevallier et al. [18] studied the structural behavior of eight commercial and industrial waxes and a heavy crude oil by X-ray diffraction. According to the experiment results, each multicomponent paraffin wax (from 20 to 33 *n*-alkanes) having a continuous distribution of consecutive *n*-alkanes ($19<n<53$), forms a single orthorhombic solid solution. The structure of this multi-alkane phase is identical to one of the two orthorhombic intermediate solid solutions, which has been observed in binary and ternary mixtures of consecutive alkanes.

The present study follows a previous investigation in our laboratory [19–23] on the thermal behavior of pure *n*-alkanes and their prepared mixtures using differential scanning calorimetry (DSC). The purpose of the present study is to provide additional phase equilibrium data for *n*-alkanes with significantly different number of carbon atoms, to characterize the thermal behavior of the binary and ternary mixtures forming immiscible systems, and to evaluate the applicability of existing empirical and semi-empirical thermodynamic models for eutectic mixtures. All three *n*-alkanes examined in this study differ considerably in chain length, which were selected to preclude complete miscibility in the solid phase, i.e. a solid solution of their mixtures would not be likely. A relatively low molecular weight *n*-alkane, $C_{16}H_{34}$, was selected to investigate the effect of a liquid *n*-alkane on two solid paraffins, one even numbered *n*-alkane, $C_{28}H_{58}$, and the other odd numbered *n*-alkane, $C_{41}H_{84}$.

2. Equilibrium (thermodynamic) models

A number of studies in the literature deal with the thermodynamic and kinetic behavior to simulate the crystallization in binary systems [9,24–31]. An 'ideal' eutectic mixture presupposes the existence of complete insolubility between the two components at all concentrations. This seldom occurs in the strictest sense; the eutectics frequently are of the non-ideal type and show the evidence of partial solubility in the solid state.

The equation describing the ideal eutectic behavior for binary mixtures is

$$\ln x_j = -\frac{\Delta H_f^0}{R}\left[\frac{1}{(T_m^E)_j} - \frac{1}{(T_m^0)_j}\right] \quad (3)$$

When mixtures deviate from the ideal behavior, mainly due to the non-zero heat of mixing, the non-ideal behavior can be accounted for by incorporating $\Delta H_m = \rho_0 x_1 x_2$, where ρ_0 is an (empirical) interaction parameter. For the case of eutectic binary systems, Lee [31] derived the following expression:

$$\frac{\rho_0(1-x_j)^2}{(\Delta H_f^0)_j} = \frac{(T_m^E)_j^*}{T_j^{ideal}} - 1 \quad (4)$$

Won [28–30] used the regular solution theory to describe the non-idealities in the oil (liquid) and wax (solid) phases. The basis of his model is the thermodynamic equilibrium between the two phases. The corresponding equation for the solid–liquid equilibrium is

$$\frac{s_j}{x_j} = \frac{\gamma_L^j}{\gamma_S^j}\exp\left[\frac{(\Delta H_f^0)_j}{R(T_m^0)_L}\left(1 - \frac{(T_m^0)_L}{(T_m^0)_j}\right) + \frac{\Delta C_P}{R}\left(1 - \frac{(T_m^0)_j}{(T_m^0)_L} + \ln\frac{(T_m^0)_j}{(T_m^0)_L}\right) + \int_0^P \frac{V_L^j - V_S^j}{RT}\,dP\right] \quad (5)$$

Pedersen et al. [9] evaluated the performance of Won's [28–30] model with extensive data on the cloud-point temperature and the amount of wax (solid) formed. To obtain an improved representation, Pedersen et al. [9] proposed a modification of Won's model. Coutinho et al. [27] developed the chain delta lattice parameter (CDLP) model for the high temperature solid phase, allowing a successful description of the solid–liquid equilibrium of *n*-alkanes.

3. Experimental

The three *n*-alkanes studied in this work were obtained from Aldrich Chemical (Milwaukee, WI, USA) and Fluka Chemie AG (New York, NY, USA).

The results described in this study, were obtained using a Mettler differential scanning calorimeter Model DSC-12E interfaced with a PC for automatic data acquisition. During all measurements, the DSC measuring cell was continuously purged with dry nitrogen. The DSC was calibrated for temperature and heat flow values using the melting point and enthalpy of fusion of high purity indium according to the standard procedures described in the user's manual.

For the DSC measurements, about 4–8 mg of each alkane was weighed to ±0.001 mg on a Mettler UMT2 microbalance directly into the aluminium crucible (sample container). The crucible was then cold-welded (mechanically sealed) to its cover using a mechanical crucible sealer. A crimp-sealed empty aluminium crucible was used as a reference in all measurements.

Samples of the three binary pairs were prepared by sealing together both alkanes in the same crucible. The total mass of alkane pairs did not exceed 8 mg. Samples of ternary mixtures were prepared by sealing together predetermined masses of all three alkanes in the same crucible. In this case, the total mass was also 8 mg or less.

Three different thermal treatment steps were employed for each sample in the study. First, to erase the thermal histories of the as-received alkanes, each prepared alkane sample was annealed initially at 120°C for at least 2 min. To examine whether vaporization had occurred at the temperature of 120°C, the total mass of the $C_{16}H_{34}$ sample and crucible was measured. No difference was found in the mass before and after the thermal treatment, ensuring that the isothermal step did not cause any vaporization of $C_{16}H_{34}$. After the 2 min isothermal step, single-component samples were cooled at the rate of 1–7°C min^{-1} to a final temperature 30°C below the melting point of the alkane. For binary and ternary mixtures, the samples were cooled at the rate of 1°C min^{-1} to a final temperature 20°C below the melting point of the shorter alkane in the mixture. The third thermal treatment was the re-heating step. Each sample was heated at a rate of 1–7°C min^{-1}, to a temperature 30°C above the melting point, for single-component samples, or 20°C above the melting point of the longer alkane in the binary and ternary mixtures. Further details of the experimental procedure have been reported elsewhere [32].

Using the procedure described by Hammami and Mehrotra [23], the liquidus temperature as well as the

eutectic temperature for binary and ternary mixtures were estimated from the melting DSC thermograms obtained at the heating rate of 1°C min^{-1}.

4. Results and discussion

4.1. Pure alkanes

The purities as well as the measured ΔH_{tot} (total phase change enthalpy) and the equilibrium melting temperature of these *n*-alkanes are reported in Table 1. Hexadecane, $C_{16}H_{34,}$ is a liquid at the room temperature whereas octacosane, $C_{28}H_{58,}$ and hentetracontane, $C_{41}H_{84}$, exist in the solid phase. The melting points, T_m^0, in Table 1, do not correspond to the peak melting points but rather to the return to the baseline temperatures [20,21]. Melting temperatures determined by DSC are compared to the values calculated using Wunderlich's formula [33], excepting $C_{16}H_{34}$ for which an extrapolation of the formula was required. The values of ΔH_{tot} are reported on molar as well as mass basis. For ΔH_{tot} of $C_{16}H_{34}$ and $C_{28}H_{58}$, a reasonable agreement is achieved between the experimental and literature values [19,35]. An interesting observation was noted concerning the measurement of ΔH_{tot} for $C_{28}H_{58}$. For the sample tested by Hammami [19], the measured average value of ΔH_{tot} for $C_{28}H_{58}$ was 90.6 kJ mol^{-1}, compared with 96.1 kJ mol^{-1} that was reported by Hammami [19]. However, as reported in Table 1, the measured value of ΔH_{tot} for a freshly acquired sample was 99.1±0.8 kJ mol^{-1}, which is in good agreement with the literature data [35]. The values of ΔH_{tot}, on a molar basis, increase with the molar mass of *n*-alkanes, which is in agreement with other studies [36–38]. Note that the theoretical values of ΔH_{tot} [34] are somewhat higher than the experimental and literature values. Dorset et al. [7] and Hammami and Mehrotra [20,21] have also reported similar findings, which have been attributed to the alkanes not being perfectly crystalline.

In this study, the equilibrium melting temperatures of pure alkanes as well as their binary and ternary mixtures were evaluated from the 1°C min^{-1} melting traces to minimize the effects of supercooling and superheating. For pure components, additional DSC thermal traces were measured at various scan rates (1, 3, 5 and 7°C min^{-1}) to study the effects of superheating and supercooling.

The heating and cooling scans for $C_{16}H_{34}$ and $C_{41}H_{84}$ are shown in Figs. 1–4. It can be seen for all measurements that the baseline is the continuation of straight lines observed on the measured DSC curves before and after the thermal event. Figs. 2 and 4 for the cooling DSC curves for $C_{16}H_{34}$ and $C_{41}H_{84}$, respectively, show that the crystallization peaks are essentially mirror images of the melting peaks in

Table 1
Melting temperatures and transition enthalpies for the three *n*-alkanes

	$C_{16}H_{34}$	$C_{28}H_{58}$	$C_{41}H_{84}$
Source	Aldrich	Aldrich	Fluka
Purity	99%	99%	>97%
T_m^0 (exp[a]) (°C)	18.8±0.2	63.1±0.3	84.3±0.2
T_m^0 (calc[b]) (°C)	13.6	60.1	82.6
ΔH_{tot} (exp[c]) (J g^{-1})	228±1	251±2	233±2
ΔH_{tot} (calc[d]) (J g^{-1})	236.9	261.6	271.8
ΔH_{tot} (exp[c]) (kJ mol^{-1})	51.6±0.2	99.1±0.8	134.5±1.2
ΔH_{tot} (lit) (kJ mol^{-1})	47.5–53.4[e]	97.1–100.2[e] 96.1[f]	
ΔH_{tot} (calc[d]) (kJ mol^{-1})	53.6	103.0	158.0

[a] Experimental (average of three to five measurements).
[b] Calculated — Wunderlich [33].
[c] Experimental using Metter Graphware TA89E package.
[d] Calculated — Dollhopf et at. [34].
[e] Literature — Domalski and Hearing [35].
[f] Literature — Hammami [19].

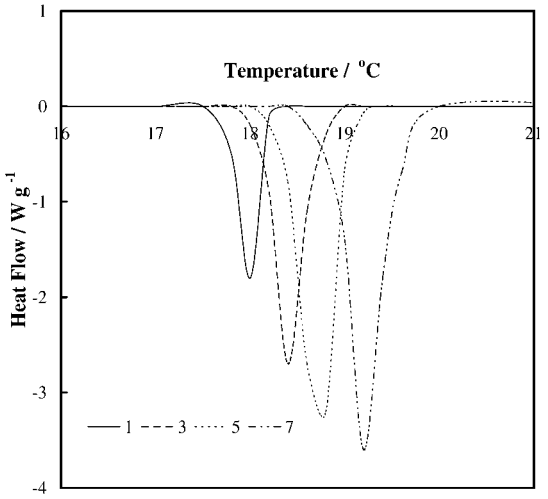

Fig. 1. Heating endotherms for $C_{16}H_{34}$ at indicated scan rates (°C min^{-1}).

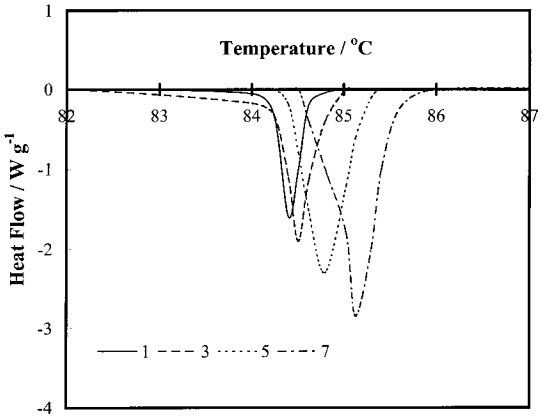

Fig. 3. Heating endotherms for $C_{41}H_{84}$ at indicated scan rates (°C min^{-1}).

Figs. 1 and 3, except that the cooling curves are shifted to slightly lower temperatures. The liquid–solid phase transformation at the cooling rate of 1°C min^{-1} occurs about 2–3°C lower than the solid–liquid phase change (i.e. the melting process) at the same scan rate. There is only one major peak representing liquid–solid transition upon cooling and/or heating regardless of the scan rate. The temperature range for melting and solidification at the scan rate of 1°C min^{-1} is found to be very narrow, less than 1°C. An increase in the scan rate brings about an increase in the peak height, accompanied with an enlarged temperature range due to the moving away of the process from thermodynamic equilibrium, e.g. at the scan rate of 7°C min^{-1} the temperature range becomes 2°C.

DSC traces at different heating and cooling scan rates for $C_{28}H_{58}$ are presented in Figs. 5 and 6. These DSC curves are quite different from those obtained for $C_{16}H_{34}$ and $C_{41}H_{84}$. The DSC curves show the existence of two major peaks. The higher temperature peak represents the hexagonal-to-melt transition and the lower temperature peak is for the orthorhombic-to-hexagonal crystalline transition, involving a rotational motion at the molecular level [4]. The observed double peak is a clear indication of the polymorphic nature of this alkane. Normal alkanes with the number of carbon

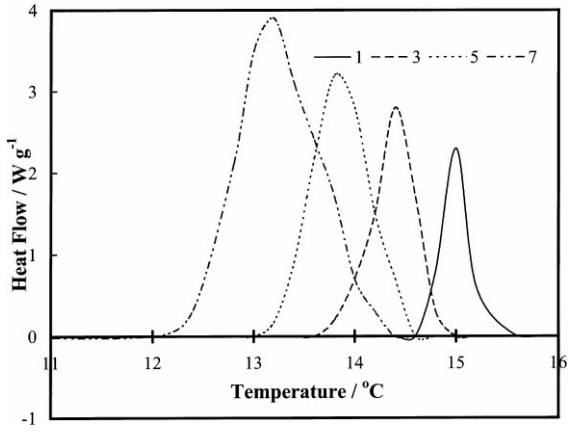

Fig. 2. Cooling exotherms for $C_{16}H_{34}$ at indicated scan rates (°C min^{-1}).

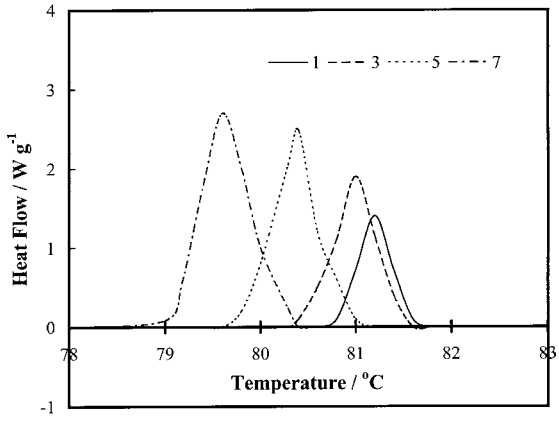

Fig. 4. Cooling exotherms for $C_{41}H_{84}$ at indicated scan rates (°C min^{-1}).

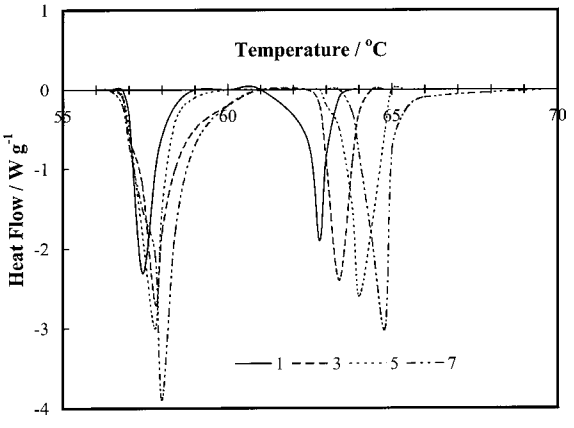

Fig. 5. Heating endotherms for $C_{28}H_{58}$ at indicated scan rates (°C min^{-1}).

atoms between 21 and 40 are known to exhibit a solid–solid transition from an orthorhombic to a hexagonal crystal structure upon heating [22]. With increasing temperature, this structure transforms, before melting occurs, into face-centered orthorhombic, the so-called rotator form [39]. This form has a large degree of rotational freedom; the molecules are supposed to oscillate around their longitudinal axis, an effect that increases with temperature [40,41].

4.2. Binary mixtures

A large number of DSC measurements were made on the three binary *n*-alkane systems, $C_{16}H_{34}$+$C_{28}H_{58}$, $C_{16}H_{34}$+$C_{41}H_{84}$ and $C_{28}H_{58}$+$C_{41}H_{84}$, at the scan rate of 1°C min^{-1}.

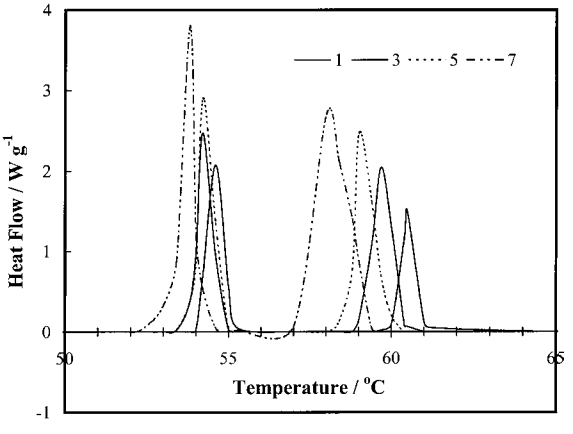

Fig. 6. Cooling exotherms for $C_{28}H_{58}$ at indicated scan rates (°C min^{-1}).

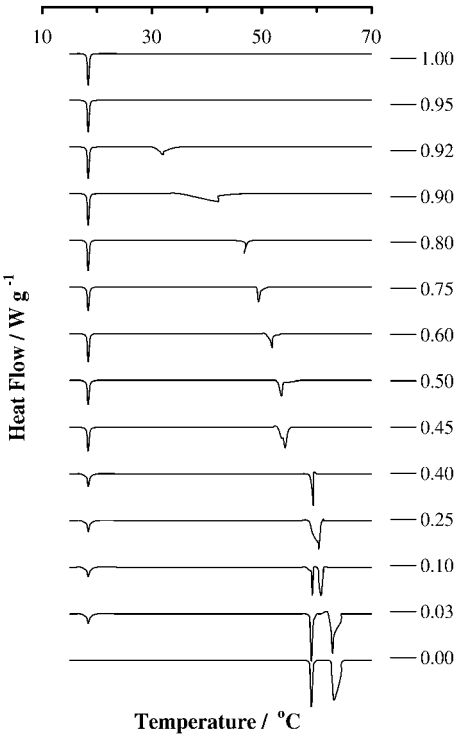

Fig. 7. Melting DSC curves of $C_{16}H_{34}$+$C_{28}H_{58}$ binary mixtures at the indicated mole fractions of $C_{16}H_{34}$.

4.2.1. DSC results for $C_{16}H_{34}$+$C_{28}H_{58}$ mixture

All presented binary measured DSC curves are arranged in the order of decreasing concentration of the mixture component with a lower molar mass. Fig. 7 presents the thermal traces for binary mixture of $C_{16}H_{34}$+$C_{28}H_{58}$ at the heating rate of 1°C min^{-1}. All mixtures except those for $C_{16}H_{34}$ mole fractions of 0.95 and 1.00 exhibit at least two peaks. The lower temperature peak is independent of the mixture composition and appears at a constant temperature, which is inferred to be the eutectic temperature. Studies on binary eutectic mixtures of alkanes have indicated that the eutectic melts within one degree of the pure hydrocarbon of shorter chain length; the eutectic mixtures usually contain 90–95% of the shorter paraffin [13,15,23].

In Fig. 7, the DSC traces for higher concentrations of $C_{28}H_{58}$ exhibit three peaks. The higher temperature

peak represents the liquid–solid transformation, the middle peak is for the solid–solid transformation, and the low temperature peak corresponds to the eutectic temperature.

The solid–solid phase transition temperature for the $C_{16}H_{34}$+$C_{28}H_{58}$ system appears to be independent of the mixture composition. Compared to the solid–solid transition temperature of the binary mixture with the transition temperature of pure $C_{28}H_{58,}$ there is practically no change in the solid–solid phase transition temperature. For pure $C_{28}H_{58,}$ the solid–solid transition occurs at 58.8°C; for the binary mixture, the temperature range is 58.9±0.1°C. From this evidence, it can be concluded that the miscibility does not occur in the solid state over the $C_{16}H_{34}$mole fraction range of 0.0–0.4.

4.2.2. DSC results for $C_{16}H_{34}$+$C_{41}H_{84}$ mixture

The DSC curves for $C_{16}H_{34}$+$C_{41}H_{84}$ mixture are presented in Fig. 8. Unlike the case of pure components, where pure $C_{16}H_{34}$ and $C_{41}H_{84}$ exhibit just one peak corresponding to the solid–liquid transformation, all mixtures except those for $C_{16}H_{34}$ mole fractions of 0.95 and 1.00 exhibit two peaks. The DSC curves are qualitatively similar to those for the $C_{16}H_{34}$+$C_{28}H_{58}$ mixture in Fig. 7. As the concentration of $C_{16}H_{34}$ increases the melting point depression for the mixture increases. More importantly, the lower temperature peak occurs at the same temperature for all compositions. From this evidence, it can be concluded that the $C_{16}H_{34}$+$C_{41}H_{84}$ mixture also forms a eutectic system.

4.2.3. DSC results for $C_{28}H_{58}$+$C_{41}H_{84}$ mixture

Fig. 9 presents the DSC curves for $C_{28}H_{58}$+$C_{41}H_{84}$ mixtures, where all DSC curves except those for $C_{28}H_{58}$ mole fractions of 0.90, 0.92, 0.95 and 1.00 show three peaks. The highest temperature peak is for the solid–liquid phase change. The two lower temperature peaks occur at constant temperatures regardless of the mixture composition. Of these two peaks, the one at the higher temperature corresponds to the eutectic temperature. Note that pure $C_{28}H_{58}$ melts at 62.9°C, and the temperature of 61.8±0.5°C for this peak is the experimentally obtained eutectic temperature of the mixture. The lowest temperature peak represents the solid–solid transformation of $C_{28}H_{58}$.

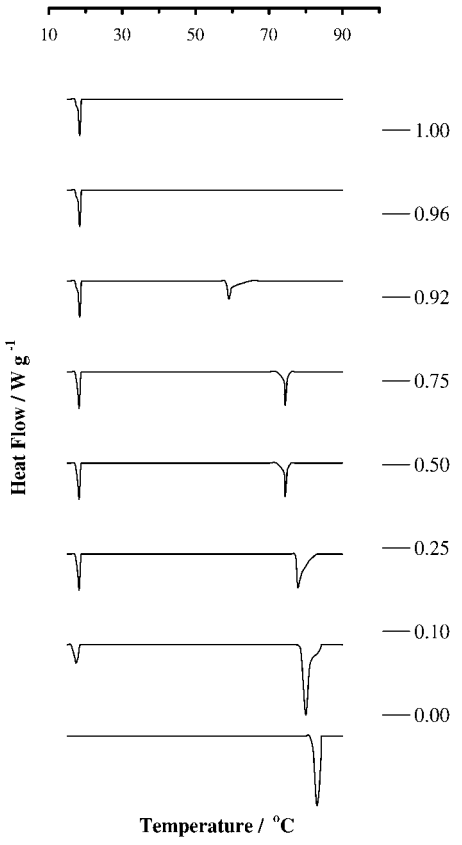

Fig. 8. Melting DSC curves of $C_{16}H_{34}$+$C_{41}H_{84}$ binary mixtures at the indicated mole fractions of $C_{16}H_{34}$.

Previous experimental studies of eutectic binary mixtures [13,23] and the $C_{16}H_{34}$+$C_{28}H_{58}$ binary mixture investigated in this study have shown that the solid–solid transitions observed in many *n*-alkanes occur at about the same temperature in their mixture. For the case of $C_{28}H_{58}$+$C_{41}H_{84}$ mixtures, however, the temperature for the solid–solid transition is lowered by about 3°C. Lowering of the solid–solid transition temperature can be explained by formation of mixed crystal in the solid phase instead of eutectic-separate extension chains. Dirand et al. [42] also reported similar findings and concluded that the behavior of binary mixtures of *n*-alkanes is far more complicated than considered in earlier studies. Instead of the appearance of one solid–solid transition, many orthorhombic intermediate phases can be detected due to the possible formation of mixed crystals.

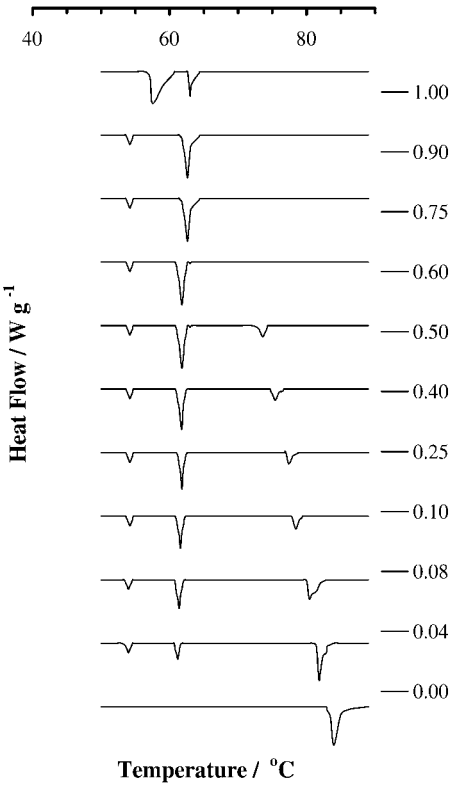

Fig. 9. Melting DSC curves of $C_{28}H_{58}$+$C_{41}H_{84}$ binary mixtures at the indicated mole fractions of $C_{28}H_{58}$.

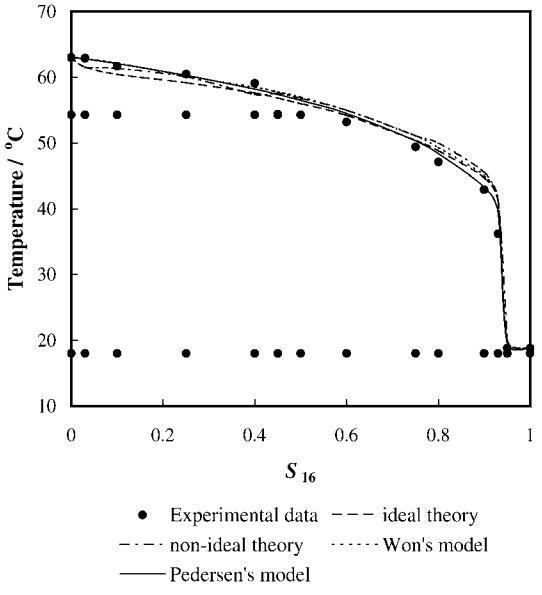

Fig. 10. Liquid–solid phase diagram for $C_{16}H_{34}$+$C_{28}H_{58}$ binary mixture; Comparison between experimental data and predictions from ideal, non-ideal, Won [28–30] and Pedersen et al. [9] models.

4.3. Binary phase diagrams

For constructing binary phase diagrams of eutectic systems, the convention of Smith and Pennings [43–45] was adopted, which uses the peak temperatures for the lower melting endotherms and the return to the baseline temperature for the higher melting endotherms. Besides the effect of undercooling, there was no difference in the shape of the phase diagram constructed from the cooling curves, compared to the one from the heating curves [32].

The data treatment for all binary mixtures involved the comparison of experimental phase diagrams with the ideal solution theory. To define the deviation from ideal eutectic behavior, the regular solution theory, Won's model [28–30] and Pedersen et al.'s model [9] were used.

Comparisons between the experimental data and models predictions for the eutectic systems are presented in the Figs. 10, 11 and 12 for $C_{16}H_{34}$+$C_{28}H_{58}$,

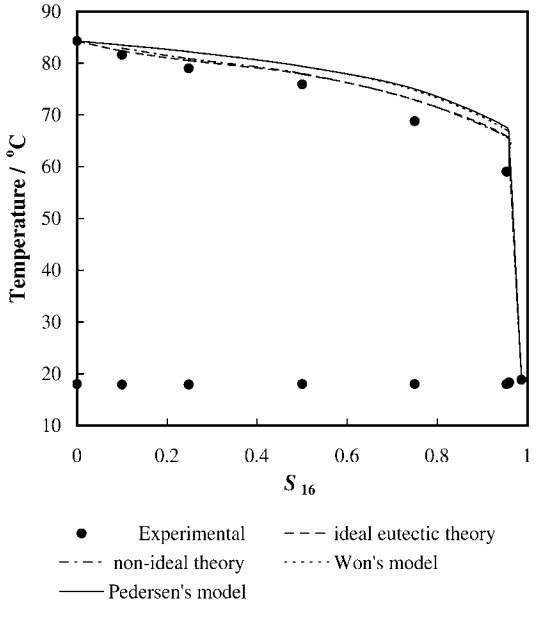

Fig. 11. Liquid–solid phase diagram for $C_{16}H_{34}$+$C_{41}H_{84}$ binary mixture; Comparison between experimental data and predictions from ideal, non-ideal, Won [28–30] and Pedersen et al. [9] models.

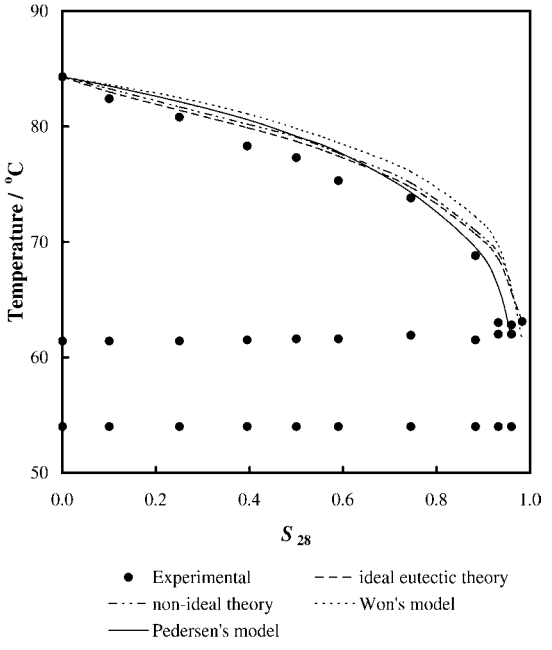

Fig. 12. Liquid–solid phase diagram for $C_{28}H_{58}$+$C_{41}H_{84}$ binary mixture; Comparison between experimental data and predictions from ideal, non-ideal, Won [28–30] and Pedersen et al. [9] models.

$C_{16}H_{34}$+$C_{41}H_{84}$ and $C_{28}H_{58}$+$C_{41}H_{84}$ systems, respectively. The results presented in the Figs. 10, 11 and 12 show that ideal solution theory, regular solution theory and Pedersen et al.'s model yield good results for the liquidus temperature, but with varying success for different mixtures. Pedersen et al.'s model gives the best fit for the $C_{16}H_{34}$+$C_{28}H_{58}$ system. Due to a large difference in the chain length between $C_{16}H_{34}$ and $C_{41}H_{84}$, the mixture of $C_{16}H_{34}$+$C_{41}H_{84}$ is best described by the ideal eutectic model. For the $C_{28}H_{58}$+$C_{41}H_{84}$ system, the mixture melting points calculated from the non-ideal model gave the best match of the experimental results. The optimum value of ρ_0 to yield the closest match to experimental results for $C_{28}H_{58}$+$C_{41}H_{84}$ mixture is 2.05 kJ mol^{-1}.

Equilibrium calculations for all three eutectic systems in this study indicated the evidence of non-idealities. In spite of the large differences in the chain length, all of the mixtures are non-ideal with varying extents of mixing in the solid state. The non-ideality is particularly significant around the eutectic composition and temperature, where instead of the formation of two separate solid phases, formation of mixed crystals could occur. The difference between experimental results and predictions from the ideal solution theory, particularly in the vicinity of the eutectic point, can probably be explained in terms of the trapping of smaller molecules by larger molecules during simultaneous solidification/crystallization.

Both Won's and Pedersen et al.'s models gave nearly the same values of the liquid phase solubility parameter throughout the range of carbon numbers, but the variation was greater in the values of the solid phase solubility parameter [32]. Any difference between the predictions from these two models can be explained in terms of the different values of solubility parameters for liquid and solid phases. Values of the solid phase solubility parameter predicted from the Pedersen et al.'s model were about 70% higher than those from Won's model. The reason for the over-prediction of temperatures by Won' model is perhaps the small value for the solubility parameter in the solid state [32]. Pauly et al. [46] performed measurements at atmospheric pressure on mixtures made up of decane and various distributions of heavy normal paraffins from octadecane to triacontane. The liquid–solid equilibrium data were compared with predictions from several models, including Won [28–30], Pedersen et al. [9] and Coutinho et al. [17]. Pauly et al. also reported that all activity coefficient models overestimate the solid appearance temperatures slightly.

For each binary mixture, the experimental results were also compared with predictions from the regular solution theory. By adjusting the empirical parameter, ρ_0, the best fit of experimental data was achieved. A total of five values of ρ_0 were available for different pairs of *n*-alkanes, i.e. three from the present study and one each from Hammami and Mehrotra [23] and Bhat [13]. For all binary mixtures, the corresponding values of the ρ_0 and the difference in the chain length, Δn, were fitted by the following correlation:

$$\rho_0 = 0.706 + \frac{19.70}{\Delta n} \tag{6}$$

It is emphasized that Eq. (6) should be used for the estimation of ρ_0 for eutectic mixtures only if the difference in chain length is outside the boundary conditions for the formation of solid solution, which are calculated from Eqs. (1) or (2).

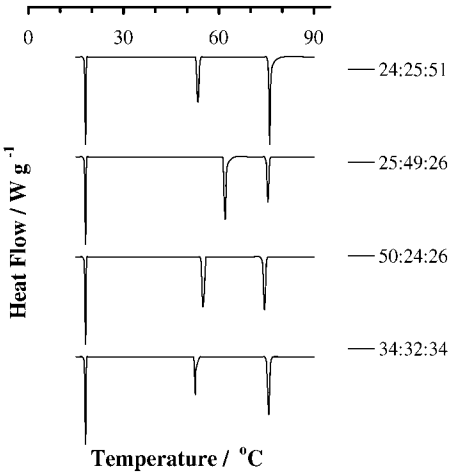

Fig. 13. Melting DSC curves of $C_{16}H_{34}$+$C_{28}H_{58}$+$C_{41}H_{84}$ ternary mixture at the indicated molar compositions (%) of $C_{16}H_{34}$, $C_{28}H_{58}$ and $C_{41}H_{84}$, respectively.

4.4. The ternary mixture

Four samples of the ternary mixture (i.e. $C_{16}H_{34}$+$C_{28}H_{58}$+$C_{41}H_{84}$) were prepared and tested on the DSC. In Fig. 13, all measured DSC curves exhibit three major peaks. The DSC traces for the $C_{16}H_{34}$+$C_{28}H_{58}$+$C_{41}H_{84}$ mixture retain qualitatively most of the thermal characteristics of the three pure *n*-alkanes. However, the peak for the solid–solid transition of $C_{28}H_{58}$ is not present in any of the DSC curves. Table 2 presents the experimental values of the phase transformation and eutectic temperatures for the ternary mixtures. The eutectic temperature in each case is about 1°C lower than the melting temperature of the shortest-chain alkane, i.e. $C_{16}H_{34}$, a result which is similar to that for binary mixtures presented earlier.

Table 2 also includes a comparison between experimental values of T_m^E for the ternary system and the predictions from thermodynamic models. The results indicate that all three models overestimate slightly the liquidus temperature. Of the three models considered, the predictions from the ideal solution theory match the experimental data the best. In general, the measurements with ternary mixtures support the results obtained on the binary mixtures, i.e. formation of eutectic mixture, but existence of mixed crystals and some solubility in the solid state. It was observed that the interactions between *n*-alkanes in the ternary system are generally the same as those in the binary mixtures [32]. Hence, the experimental results for binary mixtures should be sufficient for modelling the thermodynamic behavior of multicomponent mixtures of paraffins.

5. Conclusions

Results obtained in this study verify that the DSC technique, as a method of thermal analysis, is a sufficiently accurate tool for investigating the thermal behavior of, and the interactions between, *n*-alkanes. The DSC curves show a shift to the higher temperature as the heating rate is increased. At higher cooling

Table 2
Measured and predicted phase transition and eutectic temperatures of $C_{16}H_{34}$+$C_{28}H_{58}$+$C_{41}H_{84}$ ternary mixtures

Sample	Mixture composition (mol%)	Experimental phase transition and eutectic temperatures (°C)	Predicted values of T_m^E (°C)		
			Ideal eutectic model	Won's model [28–30]	Pedersen et al. model [9]
1	$C_{16}H_{34}$=24	T_m^E=76.0	79.8	79.4	80.1
	$C_{28}H_{58}$=25	T_β=53.4			
	$C_{41}H_{84}$=51	T_E=18.0			
2	$C_{16}H_{34}$=25	T_m^E=75.5	75.7	75.8	78.6
	$C_{28}H_{58}$=49	T_β=62.0			
	$C_{41}H_{84}$=26	T_E=18.3			
3	$C_{16}H_{34}$=50	T_m^E=74.5	75.3	75.5	78.4
	$C_{28}H_{58}$=24	T_β=55.0			
	$C_{41}H_{84}$=26	T_E=18.0			
4	$C_{16}H_{34}$=34	T_m^E=75.8	77.4	79.0	79.4
	$C_{28}H_{58}$=32	T_β=52.6			
	$C_{41}H_{84}$=34	T_E=18.0			

rates, the effect of supercooling is evident in the noticeable shift of the peaks to lower temperature. However, solid–solid transition in binary mixtures was found to occur without much influence of supercooling or superheating. All three *n*-alkane binary systems, with large differences in chain length, showed eutectic behavior; hence, a large difference in chain length is the key factor for the occurrence of immiscible solid phases.

The DSC results were evaluated with available thermodynamic models. All models were found to be highly responsive to the components in the mixture, and predicted the melting temperature accurately for at least one mixture. All models overestimate the solid appearance temperature, however, this overestimation was only slight. Also, the agreement between experimental data and model predictions was not always satisfactory, especially in the vicinity of the eutectic composition and temperature; a fact pointing to a complex non-ideal behavior of mixtures, where instead of the formation of two separate solid phases, formation of mixed crystals could occur.

It was also found that the interaction between *n*-alkanes in ternary mixtures are comparable to those in binary mixtures; hence, experimental results on binary mixtures should be sufficient for modelling the thermodynamic behavior of multicomponent mixtures of paraffins.

6. Nomenclature

ΔC_P	difference in heat capacity between liquid and solid phases
ΔH_m	heat of mixing
ΔH_{tot}	total phase change enthalpy (sum of enthalpies of liquid–solid and solid–solid transformations)
$(\Delta H_f^0)_j$	enthaply of fusion of component j
n	carbon number
n_{max}	maximum chain length
n_{min}	minimum chain length
P	pressure
R	universal gas constant
s_j	solid phase mole fraction of component j
T_E	eutectic temperature
T_m^0	equilibrium melting temperature for pure component
$(T_m^0)_L$	equilibrium liquidus temperature for isomorphous mixture
$(T_m^E)_j^*$	non-ideal liquidus temperature of component j in eutectic mixture
T_j^{ideal}	ideal liquidus temperature of component j in eutectic mixture
T_β	solid–solid phase transition temperature
V_L^j	molar volume of component j in liquid phase
V_S^j	molar volume of component j in solid phase
x_j	liquid phase mole fraction of component j

Greek symbols

γ_L^j	activity coefficient of component j in liquid phase
γ_S^j	activity coefficient of component j in solid phase
ρ_0	interaction parameter

Acknowledgements

Financial support was provided by the Natural Sciences and Engineering Research Council of Canada (NSERC) and the Department of Chemical and Petroleum Engineering, University of Calgary.

References

[1] W.J. Matlach, M.E. Newberry, SPE Paper 1151, Rocky Mountain Regional Meeting, Salt Lake City, UT, 1983.
[2] E. Gimzewski, G. Audley, Thermochim. Acta 214 (1993) 149.
[3] M.Q.S.P. Marconnelli, H.L. Strauss, R.G. Snyder, J. Am. Chem. Soc. 104 (1982) 6237.
[4] G.J. Ungar, N. Masic, J. Phys. Chem. 89 (1985) 1036.
[5] G.I. Asbach, H.G. Kilian, Polymer 32 (1991) 3006.
[6] I. Denicolo, A.F. Craievich, J. Doucet, J. Chem. Phys. 80 (1984) 12.
[7] D.L. Dorset, J. Hanlon, G. Karet, Macromolecules 22 (1990) 2169.
[8] J.M. Letoffe, P. Claudy, M.V. Kok, M. Garcin, J.L. Volle, Fuel 74 (1995) 6.
[9] K.S. Pedersen, P. Skovborg, H.P. Rønningsen, Energy & Fuels 5 (1991) 924.
[10] M.Q.S.P. Marconnelli, H.L. Strauss, R.G. Snyder, J. Phys. Chem. 89 (1985) 5260.
[11] A.I. Kitaigorskii, Organic Chemical Crystallography, Consultants Bureau, New York, 1961.
[12] R.R. Matheson, P. Smith, Polymer 26 (1985) 288.

[13] N.V. Bhat, Phase transformation and crystallization of paraffin mixtures under non-isothermal condition, M.Sc. Thesis, University of Calgary, Calgary, Canada, 1996.
[14] M. Dirand, Z. Achour, B. Jouti, A. Sabour, J.C. Gachon, Mol. Cryst. Liq. Cryst. 275 (1996) 293.
[15] W.M. Mazee, Anal. Chim. Acta 17 (1957) 97.
[16] W.R. Turner, Ind. Eng. Chem. Prod. Res. Dev. 10 (1971) 238.
[17] J.A.P. Countinho, V. Meray, Fluid Phase Equilibria 148 (1998) 147.
[18] V. Chevallier, D. Petitjean, M. Bouroukba, M. Dirand, Polymer 40 (1999) 2129.
[19] A. Hammami, Thermal behavior and non-isothermal crystallization kinetics of normal alkanes and their waxy mixtures under quiescent conditions, Ph.D. Thesis, University of Calgary, Calgary, Canada, 1994.
[20] A. Hammami, A.K. Mehrotra, Thermochim. Acta 211 (1992) 137.
[21] A. Hammami, A.K. Mehrotra, Thermochim. Acta 215 (1993) 197.
[22] A. Hammami, A.K. Mehrotra, Fuel 74 (1995) 96.
[23] A. Hammami, A.K. Mehrotra, Fluid Phase Equilibria 111 (1995) 253.
[24] R.M. Butler, D.M. MacLeod, Can. J. Chem. Eng. 39 (1961) 53.
[25] A.G. Lee, Biochim. Biophys. Acta 472 (1977) 285.
[26] W.M. Mazee, Recueil 67 (1948) 197.
[27] J.A.P. Countinho, S.I. Andersen, E.H. Stenby, Fluid Phase Equilibria 117 (1996) 138.
[28] K.W. Won, Paper 27A, AIChE Spring National Meeting, Houston, TX, 1985.
[29] K.W. Won, Fluid Phase Equilibria 30 (1986) 265.
[30] K.W. Won, Fluid Phase Equilibria 53 (1989) 377.
[31] A.G. Lee, Biochim. Biophys. Acta 507 (1978) 433.
[32] I. Paunovic, Solid–liquid phase behavior of mixtures of *n*-alkanes, M.Sc. Thesis, University of Calgary, Calgary, Canada, 1999.
[33] B. Wunderlich, Macromolecular Physics, Vol. 3, Academic Press, New York, 1980.
[34] W. Dollhopf, H.P. Grossmann, U. Leute, Colloids Polym. Sci. 259 (1981) 267.
[35] E.S. Domalski, E.D. Hearing, J. Phys. Chem. Ref. Data 25 (1996) 1.
[36] M.G. Broadhurst, J. Res. N.B.S.A. (Section A) 66A (1962) 241.
[37] M.G. Broadhurst, J. Res. N.B.S.A. (Section A) 67A (1963) 3.
[38] C.M.L. Atkinson, J.A. Larkin, M.J. Richardson, J. Chem. Thermodyn. 1 (1969) 435.
[39] P. Espeau, L. Robles, M.A. Cuevas-Dirate, D. Mondieig, Y. Haget, Mater. Res. Bull. 31 (1996) 10.
[40] R. Stolk, F. Rajabalee, M.H. Jacobs, P. Espeau, D. Mondieig, H.A.J. Oonk, Y. Haget, Calphad 3 (1997) 401.
[41] E.B. Sirota, H.E. King Jr., D.M. Singer, H.H. Shao, J. Chem. Phys. 98 (1993) 5809.
[42] M. Dirand, V. Chevallier, E. Provost, M. Bouroukba, D. Petitjean, Fuel 77 (1998) 12.
[43] P. Smith, A.J. Pennings, Polymer 15 (1974) 413.
[44] P. Smith, A.J. Pennings, J. Mater. Sci. 11 (1976) 1450.
[45] P. Smith, A.J. Pennings, J. Polym. Sci. Polym. Phys. Ed. 15 (1977) 523.
[46] J. Pauly, C. Dauphin, J.L. Daridon, Fluid Phase Equilibria 149 (1998) 191.